Journal of Applied Polymer Science

Mechanical and non-isothermal crystallization properties of coal gasification fine slag glass beads filled polypropylene composites

--Manuscript Draft--

Full Title:	Mechanical and non-isothermal crystallization properties of coal gasification fine slag glass beads filled polypropylene composites
Manuscript Number:	
Article Type:	Research Article
Order of Authors:	Weidong Ai
	Shuo Liu
	Jiupeng Zhang
	Shiding Miao
	Cundi Wei
Manuscript Classifications:	Applications; Crystallization; Mechanical Properties; Morphology; Porous Materials
Additional Information:	

Question	Response
Please provide the principal investigator's name and affiliation. (Principal investigator MUST be listed as a co-author on the submission; please DO NOT list all other co-authors in this section.)	Weidong Ai, Key Laboratory of Automobile Materials (Ministry of Education), College of Materials Science and Engineering, Jilin University, Changchun 130025, People's Republic of China
Please submit a plain text version of your cover letter here. If you also wish to upload a file containing your cover letter, please note it here and upload the file when prompted to upload manuscript files. Please note, if you are submitting a revision of your manuscript, there is an opportunity for you to provide your responses to the reviewers later; please do not add them to the cover letter.	Dear Editors: We would like to submit the enclosed manuscript entitled mechanical and non-isothermal crystallization properties of coal gasification fine slag glass beads filled polypropylene composites, which we wish to be considered for publication in Journal of Applied Polymer Science. No conflict of interest exits in the submission of this manuscript, and manuscript is approved by all authors for publication. We would like to declare on behalf of my co-authors that the work described was original research that has not been published previously, and not under consideration for publication elsewhere, in whole or in part. We acknowledge the financial supports by the Jilin Province/Jilin University Co-construction Project–Funds for New Materials (SXGJSF2017-3). In this work, the coal gasification fine slag (CGFS) was subjected to calcine at 600 °C for 7 h, which was termed as coal gasification fine slag glass beads (CGFSGB). CGFSGB was successfully incorporated into polypropylene (PP) by melt compounding. The results indicated that CGFSGB has the potential to replace calcium carbonate (CC) in plastics market. Thermogravimetric analysis showed obvious reinforcement in thermal stability by incorporation of CGFSGB, but crystallization ability decreased. The CGFSGB was modified with 3-methacryloxypropyltrimethoxy silane (KH570) and hydrochloric acid (HCl) to improve compatibility between CGFSGB and PP, CGFSGB-S and CGFSGB-A obtained respectively. The tensile strength, thermal stability and crystallization ability of PP composites and dispersity of CGFSGB were increased after the modification by KH570 and HCl, and PP/CGFSGB-A composites showed better performance compared to PP/CGFSGB-S composites. The mathematical model and SEM revealed that stabilization of tensile strength of PP/CGFSGB-A composites was attributed to existence of the mesoporous in CGFSGB-A.

	Coal gasification slag is a byproduct from the entrained flow coal gasification, which can be classified by two types, CGFS and coal gasification coarse slag according to the location of the discharge. The improper disposal of coal gasification slag has resulted in the environmental pollution. A comprehensive utilization of the waste slag is becoming an urgent issue. Efforts are being made to form value added products from the coal gasification slag. CGFSGB can be extracted from CGFS. In this work, the feasibility of CGFSGB as a filler of PP is studied. CGFSGB has higher surface reaction activity owing to its amorphous phase. A potential application of CGFSGB is as a filler in polymer matrix. But, there is rare research about this issue. It is the key result that the tensile strength of PP composites change slightly with increasing the CGFSGB-A weight fraction owing to the existence of the mesoporous. Some inorganic particles such as montmorillonite, lignin, cellulose fiber, silica, calcium carbonate, and magnesium hydroxide have been studied as the reinforcing filler for polymer. This report is original research result of broad interest to the polymer community. Due to environmental pollution and other issues, the price of general inorganic fillers such as calcium carbonate, talc powder continues to improve. The application of a new cheap inorganic filler is very meaningful. Coal gasification fine slag glass beads can replace calcium carbonate, talc, etc., used in auto parts, foam plastics, conveyor belt product. We deeply appreciate your consideration of our manuscript. And We look forward to receiving comments from the reviewers. If you have any queries, please don’t hesitate to contact me at the address below. Thank you and best regards. Yours sincerely, Name: Cundi Wei E-mail: weicundi_jlu@163.com

Mechanical and non-isothermal crystallization properties of coal gasification fine slag glass beads filled polypropylene composites

Weidong Ai, Shuo Liu, Jiupeng Zhang, Shiding Miao, Cundi Wei*

Key Laboratory of Automobile Materials (Ministry of Education), College of Materials Science and Engineering, Jilin University, Changchun 130025, People's Republic of China

Correspondence to: C. Wei (E-mail: weicundi_jlu@163.com)

ABSTRACT

The coal gasification fine slag (CGFS) was subjected to calcine at 600 °C for 7 h, which was termed as coal gasification fine slag glass beads (CGFSGB). CGFSGB was successfully incorporated into polypropylene (PP) by melt compounding. The results indicated that CGFSGB has the potential to replace calcium carbonate (CC) in plastics market. Thermogravimetric analysis showed obvious reinforcement in thermal stability by incorporation of CGFSGB, but crystallization ability decreased. The CGFSGB was modified with 3-methacryloxypropyltrimethoxy silane (KH570) and hydrochloric acid (HCl) to improve compatibility between CGFSGB and PP, CGFSGB-S and CGFSGB-A obtained respectively. The tensile strength, thermal stability and crystallization ability of PP composites and dispersity of CGFSGB were increased after the modification by KH570 and HCl, and PP/CGFSGB-A composites showed better performance compared to PP/CGFSGB-S composites. The mathematical model and SEM revealed that stabilization of tensile strength of PP/CGFSGB-A composites was attributed to existence of the mesoporous in CGFSGB-A.

INTRODUCTION

Polyolefins such as polyethylene or PP are polymer materials that are used in the textile industry for manufacturing purpose of the plastic products for daily usage such as sacks, yarns, etc[1]. PP, a thermoplastic polymeric material, is known by the outstanding cost-to-performance ratio, which has motivated the researchers to improve its properties further, for example, by reinforcement with various inorganic fillers[2-7]. The effectiveness of the general inorganic fillers in improving the mechanical and physical properties of polymers seriously depends on many factors such as aspect ratio of filler, shape, size, surface characteristics, interfacial adhesion and the degree of filler dispersion[8-11]. It has been reported that some inorganic fillers can increase the Young's modulus of polymer composites, yet cause decrease of the tensile strength and toughness[12]. This may be attributed to the stress concentration and poor filler-matrix interfacial adhesion, so how to guarantee interfacial adhesion is a key in the application of a new filler. The fillers have been widely used for the reinforcement purpose such as montmorillonite[13,14], lignin[15], silica[16], calcium carbonate (CC)[17], etc. The CC is one of the most generally used inorganic fillers in thermoplastics such as PP and polyethylene[18]. Due to environmental and pollution problems, to find a filler that can replace CC has become a hot concern.

Coal gasification slag is a byproduct from the entrained flow coal gasification, which can be classified by two types, CGFS and coal gasification coarse slag according to the location of the discharge[19]. The improper disposal of coal gasification slag has resulted in the environmental pollution. A comprehensive utilization of the waste

slag is becoming an urgent issue. The efforts have been made to prepare valuable things by filling industrial solid waste into polymer materials[20,21]. The chemical composition of CGFS is similar to that of fly ash, but the good crystalline structure leads to low activity of fly ash[22]. The modification by the silane coupling agents and acid treatment can increase the compatibility between the polymer and fly ash[22]. CGFSGB can be extracted from CGFS. CGFS has been applied in low density polyethylene[23], but the application of CGFSGB has not been found yet. The CGFSGB has higher surface reaction activity owing to its amorphous phase[23], which provides more possibility of modification. Acid-leaching treatment is expected to aid in the potential applications of coal gasification slag, resulting in the partial removal of Fe, Al and Ca, leading to surface erosion and collapse, leaving behind a framework structure possessing a larger surface area to produce the porous matter[24]. According to impurities (Fe_2O_3 and others) in fly ash, different acids have been used, such as HCl, H_2SO_4, and HNO_3, moreover, HCl is typically selected as the preferred ash pretreatment[25,26].

In this research, the CGFSGB was firstly treated by the silane coupling agent, 3-methacryloxypropyltrimethoxy silane (KH570) and hydrochloric acid (HCl), because its surface has hydrophilic siloxane and silanol groups, and its chemical composition containing metal oxides. The strong inorganic acid (HCl) compared with the silane coupling agent (KH570) were chosen to modify the CGFSGB. The effect of the modification by KH570 and HCl on the particle size, surface functional groups, morphology and other properties of CGFSGB was studied. Highly porous silica balls

were prepared from a CGFSGB precursor by HCl treatment. After surface modification, CGFSGB was used as the reinforcing filler for PP. The effects of three kinds of CGFSGB fillers and CC on the mechanical properties of PP composites were mainly studied. The effect of modification of CGFSGB on the other properties of PP was also studied.

EXPERIMENTAL

Raw materials

The primary raw materials were PP and CGFS. PP (K1840) homopolymer was used as the matrix, which was provided by China Petroleum & Chemical Corporation Beijing Yanshan Branch. The density of the PP polymer in the solid state is 0.885 g/cm^3. The CGFS with an average particle size of 21.653 μm and a specific surface area of 171.421 m^2/g was provided by China Shenhua Ningxia Coal Industry Group Co., Ltd. CGFSGB was obtained by a calcination process of CGFS in the laboratory of Jilin University. The comparative CC was provided by Guangyuan Chemical Co., Ltd (Jiangxi, China). 3-Methacryloxypropyltrimethoxy silane (KH570) and hydrochloric acid (HCl) were supplied by Dongguan Shanyi Plastic Chemical Co., Ltd. (Guangdong, China) and Beijing Beihua Fine Chemicals Co., Ltd., respectively. Other chemicals such as stearic acid, antioxidants were supplied by Aladdin Chemical Reagent Co., Ltd (Shanghai, China).

Preparation of PP/CGFSGB composites

Surface modification of CGFSGB

Before the modification experiments, the CGFS was calcined at 600 °C for 7 h (the

calcination temperature of CGFS was determined by the thermogravimertic analysis) in an air atmosphere to eliminate the carbon, which is applied as a raw material. CGFSGB was further modified by using KH570 and HCl, respectively.

About 200.00 g of desiccated CGFSGB were functionalized with 3 wt % (6 g) of KH570 according to the mass of CGFSGB in a high speed mixer (model RHP-250 A, Ronghao Industrial and Commercial Trading Co., Ltd.) under continuous high speed stirring for 1 h at a wall temperature of 110-130 °C. The KH570 was added by constant spray, which was hydrolyzed in 40 ml alcoholic water mixture (volume ratio 17:3) under ultrasound conditions for 30 min. Then the mixture was statically heated for 20 min to make the modification reaction happen fully, and cooled down to the room temperature. Finally the particles were washed with ethanol to drive off the excessive silane, and dried in oven at 85 °C for 36 h, the modified CGFSGB (CGFSGB-S) obtained. The silane coupling agent (KH570) content was chosen based on a particle dispersion analysis[22].

An appropriate amount of concentrated HCl (37 wt %) was diluted in 140 ml deionized water and put into the round-bottom flask. About 15 ± 0.01 g of CGFSGB was added there and then the flask was covered with the plastic wrap to avoid volatilization. The mixture was stirred by using a continuous mechanical stirrer in the water bath at a temperature of 70–80 °C for 3 h (pre-experiment had shown that 3 h was appropriate for the acid treatment). Then the mixture was cooled action to the room temperature. CGFSGB was separated from solution under the centrifugal force. The residue was washed thoroughly with distilled water and placed into the high

temperature oven for drying at 110 °C for 48 h. Then the CGFSGB was ground measurably and finally sealed in the transparent plastic bag for standby. The slag acidified by HCl is labeled as CGFSGB-A. The HCl concentration (3 mol/L) was chosen based on a research work done by Du and Huang[24].

Preparation

The PP composites incorporated with inorganic fillers at percentages from 5 to 40 wt % were prepared by a melting compounding technique. Firstly, four fillers (CGFSGB, CGFSGB-S, CGFSGB-A, CC) and other materials were dried in an oven at a temperature of 120 °C for 12 h to remove the moisture before melting compounding. Secondly, the filler particles were compounded with PP, lubricants and antioxidants in a high speed mixer. In the experiments, the mixtures were melting compounded in a one-step procedure using a Hartek internal mixer fitted with cam blades at a temperature of 175 °C. The mixing experiments were carried out for 5 min, and the screw speed of 30 rpm was used to produce the PP composites. The mixtures removed from above internal mixer were compression molded (using frame mould) into a plaque of 2.0 mm thick by the thermocompressor supplied by the Yuanju Machine Manufactory (Guangdong, China) at the melting temperature of 180 °C for 1.5 min under a pressure of 6 MPa. Prior to the 1.5 min compression process, the preheating was carried out for 6 min. The mould was immediately diverted to a cold press for 6 min. The compounds were punched by a sheet-punching machine supplied by the Intelligent Instrument Co., Ltd. (model CP-25, Jilin, China) to acquire the standard splines for tensile testing. For a comparison, the pure PP was prepared

by the same processing procedure.

Characterization

The results of particle size were obtained by the JL9200 laser particle size instrument (Jinan, China). The mechanical properties of PP composites were tested at room temperature. The samples were made into the dumbbell shape according to ISO/R 527–1966E. Thickness of each testing sample was metered at three different points with the digital electronic vernier caliper. The samples were tested by a Universal Materials Testing Machine (model CSS-1102C), provided by Changchun Testing Machine Research Institute. Speed of cross-head of the machine was 50 mm/min in accordance with ASTM-D638. The specimens of each group contained five independent measurements. Test result was average value of five parallel measurements. Thermogravimetric analysis (TG) was carried on the HCT-1/2 thermoanalyzer, provided by Henven Scientific Instruments Factory. The samples were heated from the air temperature to 650 °C at the rate of 10 °C/min under air atmosphere (Al_2O_3 as a inert reference). The morphology was observed by the scanning electron microscope (SEM) (model JSM-IT300LA). The tensile fractured surfaces of the PP composites were used for the SEM analysis. The melting and crystallization behaviors of the PP composites were determined by the Shimadzu differential scanning calorimetry (DSC) (model TA-60WS). The samples (approximately 5 mg) in the sealed aluminum pans were firstly melted from the room temperature to 230 °C for 3 min, and then cooled to -50 °C at 10 °C/min followed by reheating to 230 °C at the same rate for the second heating run, using

nitrogen-purged atmosphere at a rate of 50 cm^3/min. The cooling and second heating thermograms were recorded for the analysis. The calibration was carried using pure indium at the same heating rate. The X-ray diffraction (XRD) analysis of the samples was made on an X'Pert PRO X-ray diffractometer with Cu Kα radiation (λ=1.5406 Å). The measurement was carried out at 40 kV and 30 mA at a scanning speed of 2 º/min within the range of 5-40 º. The specific surface area, pore diameter and pore volume were measured by the nitrogen adsorption and desorption analysis at 77 K using a JWGB analyzer (model JW-BK222) and following the BET (Brunauer-Emmett-Teller) and BJH (Barrett-Joyner-Halenda) methods. The Fourier transform infrared spectroscopy (FTIR) spectra of the inorganic particles were obtained by a Fourier transform infrared spectrometer (Nexus-670, USA) in the range of 400-4000 cm^{-1} using the KBr pellets after 32 scans at 4 cm^{-1} resolution. Sample plates were directly put on the holder to collect spectra. The transmission electron microscope (TEM) images were captured by a transmission electron microscope (JEM-2100F, Japan) with an accelerating voltage of 10 kV. The wettability testing of inorganic particles was carried out by adding 2 g of powder to 10 ml of distilled water and then shaking for 2 min.

RESULTS AND DISCUSSION

Characteristics of CGFSGB

Distribution of particle size of CGFSGB

The distribution of particle size of CGFSGB, CGFSGB-S, CGFSGB-A and CC was summarized in Table Ⅰ and Figure 1. The average particle size of the CGFSGB was

13.161 μm, and the distribution of particle size of CGFSGB was relatively wide, mainly concentrating between 0~100 μm. After being modified by silane coupling agent (KH570), the average particle size of the CGFSGB-S was 8.382 μm, and the distribution of particle size became narrower, mainly concentrating between 0 and 50 μm. This shows that after the modification of the silane coupling agent (KH570), the dispersion of the CGFSGB particles is improved and the agglomeration is weakened, thereby the distribution of particle size is narrowed and the dispersion stability of the system is improved. Compared with the CGFSGB, the average particle size of CGFSGB-A became smaller, due to the extraction of Ca, Fe and Al by HCl. It can be easily seen that CC has the smallest average particle size, only 4.118 μm.

FTIR test results and analysis of CGFSGB

The effectiveness of modification by KH570 and HCl on CGFSGB surface was studied by FTIR analysis. A series of spectrums recorded by FTIR on the various CGFSGB particles are presented in Figure 2. As shown, the peaks at 1630 and 3440 cm^{-1} are attributed to the absorption of the -OH bending vibration, which come from water molecule in KBr[27]. The peak at 1100~1030 cm^{-1} is assigned to the asymmetric stretching vibration of the Si-O-Si (siloxane) groups, and the absorbance of Si-O-Si (siloxane) peak becomes broader and deeper for the spectrums of CGFSGB activated by silane coupling agent (KH570) and HCl as compared to CGFSGB. This may be owing to the increasing of the Si-O-Si groups after activation process. In addition, the CGFSGB has potential for modification through the peaks at 3696 and 3729 cm^{-1}, which are associated with the stretching vibration of the silanol groups (Si-OH)[28], and

their full width at half maximum is small, indicating the existence of Si-OH groups distributing regularly on the surface of CGFSGB[24]. The silanol groups (Si-OH) for CGFSGB-S and CGFSGB-A become disappeared after surface modification compared to the CGFSGB.

The modification or activation of chemical surface may be defined as the chemical bonding of molecules or molecule fragments to the surface so as to change its physicochemical properties by a controlled way. The KH570 has an advantage over other comparable organic compounds, because the silane (KH570) has potential for bonding via several mechanism[27]. The surface of CGFSGB was modified by substituting hydroxyl groups with other functional group from siliane coupling agent. The KH570 reacts with the free protons from the inorganic interphase, leading to the formation of the organic monomolecular layer on the surface of the CGFSGB. These layers are compatible and react with the organic matrix[27], which may improve the mechanical and thermal properties of the polypropylene composites.

As shown in Figure 2, the peak at 1410 cm^{-1} corresponds to the asymmetric bending vibrations of the CH_2 of olefin. The peak at 798 cm^{-1} is due to the stretching vibrations of -C=CH_2 and Si-CH_2 groups[29]. Particularly, the peak appears at around 1474 cm^{-1}, which is typical for C=O vibration in carboxylic groups[30]. The existence of the organic characteristic peaks indicates that the KH570 was introduced into surface of the CGFSGB, but these organic characteristic peaks are relatively weak. It may be owing to the small amount of KH570 used in this system. Additionally, the peak at 976 cm^{-1} is associated with the bending vibration of the Si-O (H.....H_2O),

demonstrating that Al, Fe and Ca are dissolved after the acid treatment.

Surface area and pore structure of CGFSGB

Some coarse surface and new cavities can appear after the HCl treatment as Al, Fe, Ca, and other acid-soluble matters are dissolved[26]. Table Ⅱ and Figure 3 indicates that the HCl treatment would make more mesopores and larger pore volume. Moreover, the specific surface area of CGFSGB-A increases 18 times, compared to the CGFSGB. Generally speaking, the large specific surface area filler has a large contact area with the polymer matrix, leading to a large number of bonding points and a strong binding force, therefore one would expect to acquire higher interface bonding between polypropylene and CGFSGB and improved mechanical properties of PP/CGFSGB composites resulting from rougher physical surface and larger specific surface area. In summary, CGFSGB-A can be defined as a disordered mesoporous material.

Morphology analysis of CGFSGB

The Transmission Electron Microscopy (TEM) images of CGFSGB (a, b) and CGFSGB-A (c, d) are shown in Figure 4. It is observed that the particles of CGFSGB were spherical with smooth surface, whereas CGFSGB-A was coarse. The CGFSGB-A showed a highly porous surface with the size of majority of the pores between 2 and 10 nm (Figure 3). The elemental analysis results are summed in Table Ⅲ. The mental content decreased significantly in the CGFSGB-A. This finding indicated that metallic oxides were dissolved after the acid treatment.

Figure 5 shows that the CGFSGB-S remained spherical and unbroken after the

CGFSGB was modified by KH570. As such, their properties of filling and dispersion were retained. It can be clearly seen that the sphere surface of CGFSGB-S was very coarse, compared to the CGFSGB. Therefore, the CGFSGB-S surface had a potential to contain the reactive groups.

Surface wettability analysis

To a certain degree, the wettability property of inorganic fillers in the water shows the compatibility between inorganic fillers and the polymer matrix. Figure 6 shows the wettability properties of CGFSGB, CGFSGB-S and CGFSGB-A particles in polar water. It can be clearly seen that the surface modification by the KH570 largely increased the hydrophobic property of CGFSGB in polar water. This result may be illustrated by the polarity theory. CGFSGB is polar and hydrophilic. Hence, CGFSGB was fully compatible with the water. CGFSGB became apolar and hydrophobic after the surface modification by KH570, thus CGFSGB-S was completely repelled with the water. CGFSGB-A was fully compatible with the water, demonstrating that the surface activation by HCl did not change the polar and hydrophilic properties of CGFSGB.

Tensile properties

Tensile stress versus strain curves

Figure 7(a) shows the tensile stress versus strain curves of neat PP and the PP/CGFSGB composites with different filler loadings. It can be obviously seen that the maximum tensile stress and the tensile elongation at break decrease with increasing CGFSGB weight fractions. It is worth noting that CGFSGB has a reinforcing effect when the weight fraction is 5 wt %. Figure 7(b) presents the tensile stress versus

strain curves of the PP/CGFSGB-S composites. Similar to the results displayed in Figure 7(a), it can be clearly seen that values of the maximum tensile stress and the tensile elongation at break decrease with the increasing CGFSGB-S weight fractions. However, the maximum tensile stress is rather higher than the results displayed in Figure 7(a), and the values of the tensile elongation at break are somewhat lower than the values of the results shown in Figure 7(a). Figure 7(c) displays the tensile stress versus strain curves of the PP/CGFSGB-A composites. It can be obviously observed that the maximum tensile stress does not change much, and the tensile elongation at break decreases with the increasing CGFSGB-A weight fractions. The values of the tensile elongation at break are somewhat lower than those of the results displayed in Figures 7(a) and 7(b). This illustrates that there is an obvious effect of the surface modification and activation on the tensile properties of the PP/CGFSGB composites. Figure 7(d) displays the tensile stress versus strain curves of the PP/CC composites. As can be seen from the Figure 7(d), the values of the maximum tensile stress of the PP/CC composites are lower than those of the PP/CGFSGB composites, and the values of the tensile elongation at break of the PP/CC composites are higher than those of the PP/CGFSGB composites. This shows that the reinforcement effect of CGFSGB is better than CC, which is a widely used inorganic filler.

Tensile strength

The tensile strength is a momentous parameter for characterizing the properties of the composites under tensile load[31]. It is generally thought that the tensile strength

of the composites depends, to a large great extent, on the interfacial adhesion between the inorganic filler and the polymer matrix. The better interfacial adhesion leads to the higher tensile strength of the polymer composites[23]. In this section, the comparison of tensile strength between CGFSGB, CGFSGB-S, CGFSGB-A and CC filled PP composites at different filler content is discussed. The tensile strength of the PP composites as a function of filler weight fraction is displayed in Figure 8. It can be seen that the tensile strength significantly decreases with the increasing CGFSGB, CGFSGB-S and CC weight fractions, but the tensile strength of PP/CGFSGB-S composites is somewhat higher than those of PP/CGFSGB composites, and it can be noted that none of the specimens filled by CC has the tensile energy values higher than those of other PP composites at the same filler concentration. This illustrates that the tensile strength of the PP/CGFSGB composites increases after the surface modification by KH570, and the reinforcing effect of CGFSGB is better than that of CC as shown in Figure 8. It is worth noticing that the loading of the CGFSGB and CGFSGB-S into the PP can enhance the tensile of the PP composites in the case of lower filler concentration, and the composite with CGFSGB treated by KH570 at 5 wt % filler concentration provides the highest tensile strength value among the systems. It can be clearly observed from Figure 8 that the tensile strength of the PP/CGFSGB-A composites changes slightly with increasing the CGFSGB-A weight fractions. The reason may be that the degree of interfacial adhesion between the CGFSGB-A particles and the PP matrix is the relatively good except for the PP matrix strength, and the interface could transfer effectively somewhat tensile load, leading

to the tensile strength changing slightly with increasing the filler weight fractions[23,31,32]. This shows that the interfacial adhesion between the inorganic fillers and the matrix increases after the surface activation by HCl.

The tensile strength of the polymeric composites is closely related to the interfacial adhesion between the filler and the polymer matrix. Thus, accessing the interfacial adhesion status is an important point for evaluation of the tensile strength. The above experimental results have been analyzed by the mathematical model. Turcsanyi Model can indicate the dependence of composition of tensile strength[33].

$$\sigma = \sigma_m \frac{1-\Phi_f}{1+2.318\Phi_f} exp^{B\Phi_f} \quad (1)$$

In the above eq. (1), where σ, σ_m is the tensile strength of the PP composites and the pure PP, respectively. The B is a parameter that is related to the interfacial adhesion. In general, a higher B value illustrates the stronger adhesion between the fillers and the matrix. It was observed by Bliznakov that the polymeric composite without interfacial adhesion shows a B value of 0.25[33]. With values of B increasing, the degree of interfacial adhesion is strengthened as the exponential function in eq. (1). The volume fraction (Φ_f) of fillers has been determined by the eq. (2) given below. In the eq. (2), w_i and ρ_i are the weight fraction and the density of component i, respectively. Here, the density values of PP, CGFSGB, CGFSGB-S, CGFSGB-A, CC and the assistant have been taken as 0.885, 2.28, 2.28, 1.93, 2.79 and 0.941 g/cm^3, respectively.

$$\Phi_f = \frac{w_i/\rho_i}{\sum w_i/\rho_i} \quad (2)$$

This model can well illustrate our prepared PP composites (see Figure 9). In the case

of CGFSGB, *B* value was computed to be 1.78 by the iterant trials to match the experimental results. For the CGFSGB-S, the B value is about 1.90, which indicates that the interfacial adhesion between CGFSGB-S and PP is somewhat better than that of between PP and CGFSGB. This further proves that silane coupling agent with the active groups can strengthen the interfacial adhesion between the fillers and the polymer matrix. In the CGFSGB-A filled case, *B* value is 3.24, which means that the interfacial adhesion between CGFSGB-A and PP is much better than that of other PP composites in this case. As can be seen from the infrared analysis above, the Si-O (H.....H_2O) groups exist in the surface of CGFSGB-A. In general, the presence of hydroxyl groups results in a decrease in tensile strength[27], but the CGFSGB-A composites show the best tensile performance owing to the existence of mesopores. The mesopores can provide much active spots and embedded space by the macromolecular chains of the polymer matrix, which improves the interfacial adhesion between the CGFSGB and the polymer matrix. This can also explain the better tensile strength of CGFSGB-A filled polymer. In the case of CC, *B* value was calculated to be 1.21. This illustrates that the interfacial adhesion of the CGFSGB composites is better than that of the CC composites. As stated above, the CGFSGB has a potential to substitute CC as a common industrial filler.

Tensile elongation at break

Failure strain in tensile experiment can be correlated to the fracture behavior of the polymer composites. Generally speaking, the incorporation of the inorganic fillers usually deteriorates the grade of strain at failure[34]. Figure 10 presents the

relationship between the elongation at break of the PP composites and the fillers weight fraction. It can be clearly observed that the elongation at break decreases sharply when the fillers weight fraction is lower than 5 wt %, and then decreases slightly with increasing the fillers weight fractions. It is widely known that the loading of the inorganic filler particles would reduce the integrity of the polymer matrix, and the ductility of the polymer composites would be weakened, resulting in decreasing the tensile elongation at break[31]. It is worth noticing that the tensile elongation at break of the PP composites decreases with increasing the interfacial adhesion (*B*). The stronger adhesion between the fillers and the matrix leads to the more losses in the ductility of the composites[35,36]. This illustrates that the activation process can increase the interfacial adhesion and reduce the tensile elongation at break.

It can also be observed in Figure 11 that the values of the elongation at break decrease approximately linearly with increasing the filler weight fractions except for the pure PP for the same additive. It was seen by further analysis that the correlation between the elongation at break of the composites and the fillers weight fraction can be expressed through the following equation:

$$E_t = \lambda_0 + \lambda_1 \phi_f \qquad (3)$$

Where E_t and ϕ_f are the elongation at break and the filler weight fraction respectively, and λ_0 and λ_1 are parameters determined by the tensile properties. Parameter λ_1 illustrates the sensitivity of the elongation at break to the filler weight concentration. Values of λ_0 and λ_1 could be calculated by linear regression analysis from the experimental data. Values of λ_0 and λ_1 under the experimental conditions

are showed in Table Ⅳ. It was clearly found that values of the linear regression coefficient are higher than 0.59.

Morphological analysis of the composites

It is generally thought that the mechanical strength of the polymeric composites depends closely, not only on the interfacial strength between the two phases, but also on the dispersity of the inclusions in the polymeric matrix. The dispersion state of the filler particles in the polymer matrix was characterized by means of the SEM in the research. Figure 12 is the SEM images of the tensile fracture surface of the PP composites with the fillers weight concentration of 20 wt %. In Figure 12a, the distribution of the CGFSGB particles was stripped, and they were severely agglomerated in the PP matrix. This phenomenon indicated the poor compatibility between the CGFSGB particles and the PP matrix. However, the CGFSGB-S was embedded and dispersed evenly in the PP matrix (Figure 12b). Moreover, it is found that there are some filaments on the tensile fracture surface of the PP/CGFSGB-S composite owing to generating larger shear deformation to absorb larger tensile deformation energy[37]. This result indicated that the compatibility between the CGFSGB and PP matrix was improved effectively after modification by the KH570. The reason is that the KH570 could react with the PP matrix and enhance the interfacial adhesion between the two phases. The CGFSGB-S was dispersed uniformly, and having more CGFSGB-S that could act as the effective nucleating agents was beneficial to the formation of the crystalline structure and the enhancement of the properties of the PP composites.

Figure 12c shows the morphology of the tensile fracture surface of the PP/CGFSGB-A composites. It can be observed that the distribution of the CGFSGB-A particles in the PP matrix is roughly even, and the CGFSGB-A particles are embedded in the matrix. Furthermore, the fracture surface of the composites shows CGFSGB-A particles entangled with the PP matrix in the interface of the two phases. This illustrates that the interfacial adhesion strength between the CGFSGB-A particles and the PP matrix is good. The reason is that mesoporous structure of the CGFSGB-A particles can contain macromolecular chains of the polymer. Therefore, the tensile strength changes slightly with the increasing CGFSGB-A weight fractions. Figure 12d shows the tensile fracture micrograph for the PP/CC blend containing 20 wt % calcium carbonate. The CC particles also were stripped and severely agglomerated in the PP matrix. Crazing of the PP matrix with pockets of extended voids created by cavitation of the CC indicates terrible affinity between CC and PP. The result suggests the terrible compatibility between the CC particles and the PP matrix. The sharp edges and corners of calcium carbonate can cut and block the macromolecular chains of the PP, compared to the spherical CGFSGB particles. Therefore, the values of tensile strength of the composites filled by the CGFSGB are higher than those of the composites filled by the CC.

Thermogravimetric analysis

Figure 13 and Table Ⅴ show the thermal characteristics of the PP composites with the fillers weight fraction of 20 wt %. Figure 13 illustrates that the introduction of CGFSGB particles significantly increased T_{-10} (the temperature of the total mass loss

at ten percent), T_{-50} (the temperature of the total mass loss at fifty percent), T_{max} (the temperature for the maximum weight loss) and residues at 650 °C, and decreased the mass loss (250–400 °C). Therefore, the CGFSGB particles can enhance the thermal stability of the PP composites. The decomposition temperature of the CGFSGB was higher than that of the PP matrix, because the CGFSGB particles were inorganic particles. Moreover, the CGFSGB impeded the chain-segment motion of PP. These features of the CGFSGB particles can enhance the thermal stability of PP at high temperature. Table Ⅴ demonstrates that modification by the KH570 and activation by the HCl of the CGFSGB particles can improve the thermal stability of the PP composites, compared to the unmodified CGFSGB particles. A good interfacial adhesion admits inorganic particles to act as limitation sites for the movement of the polymer chains, which makes the degradation of the polymer macromolecular chains more difficult[38]. And the mesopores in the CGFSGB-A particles prevent the spread of volatile productions throughout the PP composites in the composite decomposition stage. Therefore, the improvement of the interfacial adhesion leads to the enhancement of the thermal stability.

Crystallization and melting behaviors of the PP/CGFSGB blends

The PP is a semi-crystalline polymeric resin, and the inorganic filler particles could play a part of heterogeneous nucleation in PP matrix. The type and degree of crystallization of the PP will be altered by addition of the inorganic filler particles, leading to the variation of the mechanical properties of the composites. Figures 14 and 15 display the cooling and second heating curves of differential scanning

calorimeter of pure PP and the PP/CGFSGB composites with the fillers weight fraction of 20 wt %, respectively. The pure PP contains T_c (the crystallization peak temperature) of 116.83 °C, showing a relatively wide crystallization peak. It is found in Figure 14 that the T_c of the PP composites decreased significantly owning to the addition of the CGFSGB content, which indicates that the crystallizability of PP in the PP composites decreased with the incorporation of CGFSGB. In PP/CGFSGB blends, the heterogeneous nuclei present in PP matrix diffuses in the other phase so that the beginning of the crystallization of the PP is delayed[39]. The addition of the CGFSGB could not only function as the nucleating sites but also produce confined spaces for crystallization of PP. The nucleating sites are useful for promoting crystallization, whereas confined spaces could limit macromolecular mobility of PP to weaken crystallization. In this study, confined spaces play a major role when the CGFSGB weight fraction is 20 wt %, leading to the weakening of crystallizability. Through the above analysis, the compatibilities between the fillers and the PP matrix are different. The order of the crystallizability from low to high between the different PP composites is PP/CGFSGB < PP/CGFSGB-A < PP/CGFSGB-S, which suggests that the improvement of the interfacial adhesion and the dispersity results in the improvement of the crystallizability. The crystal structure significantly affects the mechanical and the thermal properties of the composites. When the crystal structure is relatively good, their mechanical and thermal properties are enhanced.

From Figure 15, a endothermic temperature peak at 147.87 °C was obtained for the pure PP, which was attributed to the melting of the PP crystalline phase. It can be

observed that all the composites exhibit lower T_m (the melting peak temperature), compared to the pure PP. The clear shoulder-peak in the high temperature side of melting peak appears in the second heating curves of PP/CGFSGB blends, which always occurs in lower crystallization temperature of the PP. The addition of the CGFSGB particles decreases the perfection of PP crystalloids, resulting in lower melting temperature[39]. It is well known that the PP mainly has three crystal forms: monoclinic α-phase, hexagonal β-phase and orthorhombic γ-phase. It is found clearly from Figure 15 that the prepared pure PP contains the α-crystal and the β-crystal, but the addition of the CGFSGB particles results in the disappearance of β-crystal. There is an clear β-crystal melting peak near 137 °C in the pure PP. This illustrates that the addition of the CGFSGB particles is an efficient method to obtain the pure α-PP. A possible reason for this result would be connected to the different Bravais lattice of β-PP and the CGFSGB particles[40]. Because the PP is semi-crystalline polymeric resin, but the CGFSGB particles are almost amorphous, which can't support epitaxial polymer crystallization on the CGFSGB particles surfaces[23,41].

X-ray diffraction analysis

X-ray diffraction analysis was used as an effective method to study the effect of CGFSGB on the crystal structure of PP, which suggests the information on structural quality evolution. Figure 16 shows the WAXD spectra of the pure PP and the PP composites with the fillers weight fraction of 20 wt % after crystallization at a cooling speed of 10 °C/min from 230 °C to -50 °C. It can be found that the WAXD reflections of all the samples show the typical α-monoclinic structures, and (040) diffraction of

the PP is the most intense. For the neat PP, there exists an extra diffraction at 2θ of 15 °, which may be accounted for (300) lattice planes of the hexagonal β-PP[39]. However, there are no clear reflections at 2θ of 15 ° in the X-ray reflections of the other samples. The results are in good accordance with the DSC results. The positions of the other diffraction peaks retained unchanged after the addition of the CGFSGB, which suggested that addition of CGFSGB into PP does not influence the chief crystal structure of PP.

CONCLUSIONS

In this research, the polypropylene/CGFSGB composites were prepared, and its mechanical and thermal properties were analyzed. Thermogravimetric analysis indicated that the CGFSGB improved the temperature of thermal decomposition and the residual amount of PP at high temperatures. This result was attributed to the higher thermal stability of the CGFSGB. The tensile strength and the tensile elongation at break significantly decreased with the increasing CGFSGB. The reinforcing effect of CGFSGB is better than that of CC. Therefore the CGFSGB has the potential to replace calcium carbonate in the plastics market.

The SEM and TEM revealed that the CGFSGB-S and CGFSGB-A retained the spherical shape of the CGFSGB during preparation. The effects of the KH570 and HCl treatment on the structure and composition of the CGFSGB were comprehensively studied, respectively. The modification or activation process has been successfully achieved on the CGFSGB surface. Compared to the untreated CGFSGB, a significant improvement in specific surface area and the pore volume of CGFSGB-A is found, and

the distribution of the pore is concentrated at the mesoporous. It can be found that the extracting of the metal oxides is in favor of formation of the mesoporous, and the CGFSGB-A can serve as a satisfactory mesoporous material for use.

The tensile strength, thermal stability and crystallization ability of the PP composites were improved after the modification by the KH570 and the activation by the HCl, and the CGFSGB particles treated by the HCl showed better performance in the PP composites as compared to the KH570 silane coupling agent. This illustrates that the effect of morphology is more important than that of the surface functional groups. The SEM analysis illustrated that the modified CGFSGB dispersed uniformly in the PP matrix, resulting in a homogeneous embedded structure. The modification and activation can increase the interfacial adhesion, and the tensile strength increased and the tensile elongation at break decreased with the increasing interfacial adhesion. The results showed that the values of the elongation at break decreased approximately linearly with increasing the four fillers weight fractions except for the pure PP. All of the results suggested that CGFSGB, CGFSGB-S and CGFSGB-A could be the promising material to prepare the filler products in the plastics industry.

ACKNOWLEDGEMENTS

We acknowledge the financial supports by the Jilin Province/Jilin University Co-construction Project–Funds for New Materials (SXGJSF2017-3).

REFERENCES

1. Almeida, L. A.; Marques, M. d. F. V.; Dahmouche, K. *J. Appl. Polym. Sci.* **2018**, 135, 45587.

2. Zhang, Y.; Song, Y.-Z.; Yuan, J.-J.; Yin, X.; Sun, C.-C.; Zhu, B.-K. *J. Appl. Polym. Sci.* **2018**, 135, 46423.

3. Liu, J.; Yu, Z.; Shi, Y.; Chang, H.; Zhang, Y.; Luo, J.; Lu, C. *Polymer Degradation And Stability* **2014**, 103, 83-95.

4. Zhang, Y.; Jiang, X.; Bai, Z.; Wang, J.; Qian, Z.; Liu, Y. *J. Appl. Polym. Sci.* **2018**, 135, 46066.

5. Al Imran, K.; Lou, J.; Shivakumar, K. N. *J. Appl. Polym. Sci.* **2018**, 135, 45833.

6. Subramaniam, M.; Sharma, S.; Gupta, A.; Abdullah, N. *J. Appl. Polym. Sci.* **2018**, 135, 46028.

7. Varghese, A. M.; Rangaraj, V. M.; Mun, S. C.; Macosko, C. W.; Mittal, V. *Industrial & Engineering Chemistry Research* **2018**, 57, 7834-7845.

8. Cui, L.; Wang, P.; Zhang, Y.; Zhou, X.; Xu, L.; Zhang, L.; Zhang, L.; Liu, L.; Guo, X. *J. Appl. Polym. Sci.* **2018**, 135, 45768.

9. Zhang, H.-x.; Park, J.-H.; Yoon, K.-B. Composites Science And Technology **2018**, 154, 85-91.

10. Fonseca, F. M. C.; Patricio, P. S. O.; Souza, S. D.; Orefice, R. L. *J. Appl. Polym. Sci.* **2018**, 135, 46636.

11. Lu, L.; Guo, N.; Qian, X.; Yang, S.; Wang, X.; Jin, J.; Shao, G. *J. Appl. Polym. Sci.* **2018**, 135, 45962.

12. Kamphunthong, W.; Hornsby, P.; Sirisinha, K. *J. Appl. Polym. Sci.* **2012**, 125, 1642-1651.

13. Morawiec, J.; Pawlak, A.; Slouf, M.; Galeski, A.; Piorkowska, E.; Krasnikowa, N.

European Polymer Journal **2005**, 41, 1115-1122.

14. Hwu, J. M.; Ko, T. H.; Yang, W. T.; Lin, J. C.; Jiang, G. J.; Xie, W.; Pan, W. P. *J. Appl. Polym. Sci.* **2004**, 91, 101-109.

15. de Oliveira, D. R.; Nogueira, I. d. M.; Nogueira Maia, F. J.; Rosa, M. F.; Mazzetto, S. E.; Lomonaco, D. *J. Appl. Polym. Sci.* **2017**, 134, 45498.

16. Geng, C.; Zhang, Q.; Lei, W.; Yu, F.; Lu, A. *J. Appl. Polym. Sci.* **2017**, 134, 45544.

17. Chen, T.; Lin, H.; Zhao, H.; Chen, X.; Wu, T.; Li, G.; Ji, H.; Sha, J.; Ma, Y.; Xie, L. *J. Appl. Polym. Sci.* **2017**, 134, 45535.

18. Ruiz, F. A. *Journal Of Plastic Film & Sheeting* **2000**, 16, 134-140.

19. Pan, C.; Liang, Q.; Guo, X.; Dai, Z.; Liu, H.; Gong, X. *Energy & Fuels* **2016**, 30, 1487-1495.

20. Deepthi, M. V.; Sharma, M.; Sailaja, R. R. N.; Anantha, P.; Sampathkumaran, P.; Seetharamu, S. *Materials & Design* **2010**, 31, 2051-2060.

21. Mostafa, A.; Lucyshyn, T.; Holzer, C.; Flachberger, H.; Oefner, W.; Riess, G.; Fritz, B. *J. Appl. Polym. Sci.* **2018**, 135, 46535.

22. Luo, F.; Wang, S.; Xue, B.; Jiang, Y.; Wei, C. *J. Appl. Polym. Sci.* **2013**, 129, 1053-1059.

23. Ai, W.; Xue, B.; Wei, C.; Dou, K.; Miao, S. *J. Appl. Polym. Sci.* **2018**, 135, 46203.

24. Du, M.; Huang, J.; Liu, Z.; Zhou, X.; Guo, S.; Wang, Z.; Fang, Y. *Fuel* **2018**, 224, 178-185.

25. Panitchakarn, P.; Laosiripojana, N.; Viriya-umpikul, N.; Pavasant, P. *Journal of the Air & Waste Management Association* **2014**, 64, 586-596.

26. Lee, Y.-R.; Soe, J. T.; Zhang, S.; Ahn, J.-W.; Park, M. B.; Ahn, W.-S. *Chemical Engineering Journal* **2017**, 317, 821-843.

27. Lin, O. H.; Md Akil, H.; Ishak, Z. A. M. *Polymer Composites* **2009**, 30, 1693-1700.

28. Al-Ghouti, M. A.; Khraisheh, M. A. M.; Allen, S. J.; Ahmad, M. N. *Journal of Environmental Management* **2003**, 69, 229-238.

29. Zhang, C.; Zhang, C.; Huang, R.; Gu, X. *J. Appl. Polym. Sci.* **2017**, 134, 44778.

30. Geng, W.; Nakajima, T.; Takanashi, H.; Ohki, A. *Fuel* **2009**, 88, 139-144.

31. Liang, J.-Z. *Polymer Testing* **2017**, 60, 110-116.

32. Liang, J.-Z. *Polymer Composites* **2011**, 32, 821-828.

33. Bliznakov, E. D.; White, C. C.; Shaw, M. T. *J. Appl. Polym. Sci.* **2000**, 77, 3220-3227.

34. Wu, C. L.; Zhang, M. Q.; Rong, M. Z.; Friedrich, K. *Composites Science And Technology* **2002**, 62, 1327-1340.

35. Zeng, R.-T.; Hu, W.; Wang, M.; Zhang, S.-D.; Zeng, J.-B. *Polymer Testing* **2016**, 50, 182-190.

36. Wang, M.; Deng, X.-Y.; Du, A.-K.; Zhao, T.-H.; Zeng, J.-B. *RSC Advances* **2015**, 5, 73146-73154.

37. Liang, J.-Z. *Polymer Testing* **2017**, 60, 381-387.

38. Yang, F.; Nelson, G. L. *Polymers for Advanced Technologies* **2006**, 17, 320-326.

39. Shen, H.; Wang, Y.; Mai, K. *Thermochimica Acta* **2007**, 457, 27-34.

40. Velasco, J. I.; Morhain, C.; Martinez, A. B.; Rodriguez-Perez, M. A.; de Saja, J. A. *Polymer* **2002**, 43, 6813-6819.

41. Hooks, D. E.; Fritz, T.; Ward, M. D. *Advanced Materials* **2001**, 13, 227-241.

Figure 1. The distribution of particle size of CGFSGB, CGFSGB-S, CGFSGB-A and CC.

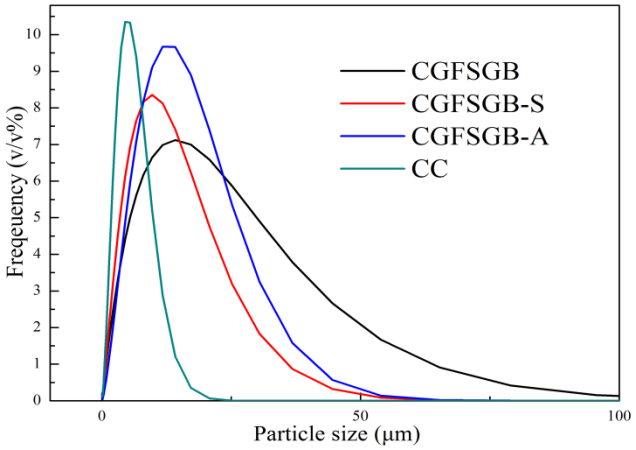

Figure 2. The FTIR spectra of CGFSGB, CGFSGB-S and CGFSGB-A.

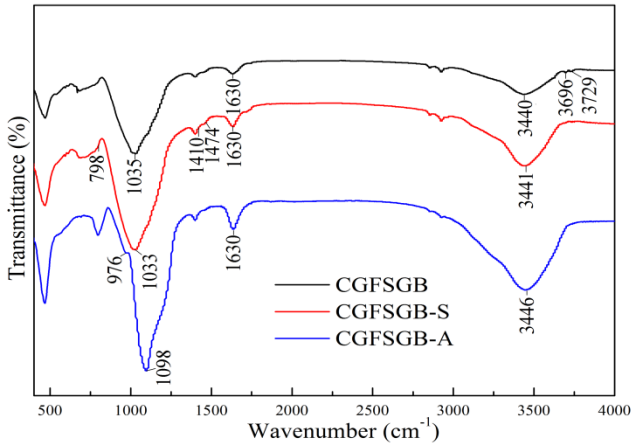

Figure 3. Pore size distribution and adsorption/desorption isotherms of CGFSGB and CGFSGB-A.

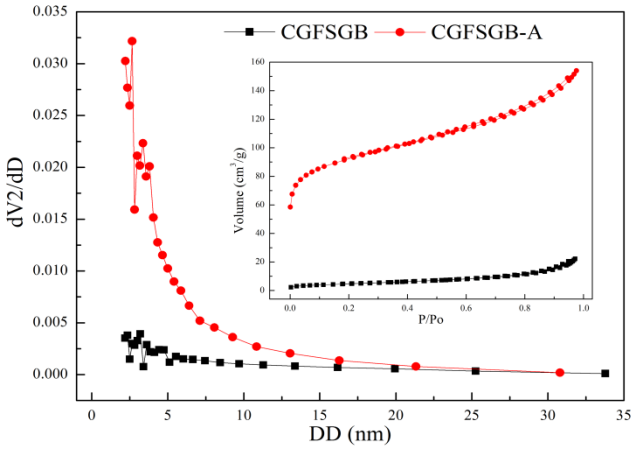

Figure 4. The TEM images of CGFSGB (a, b) and CGFSGB-A (c, d).

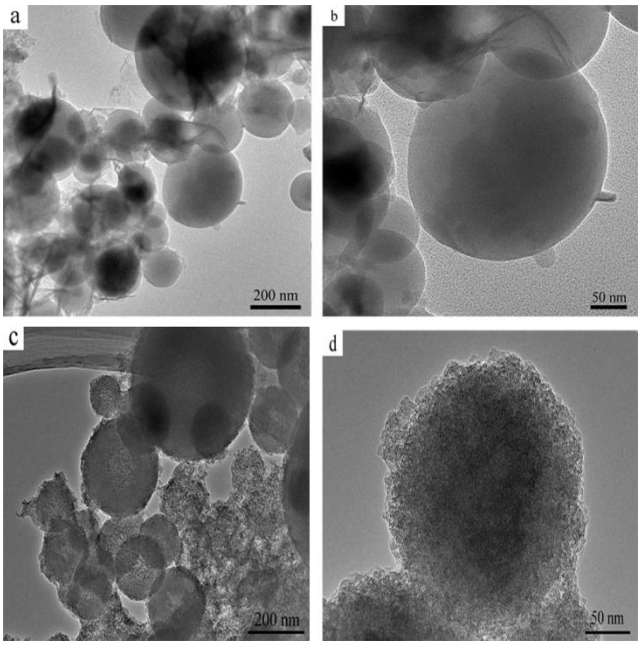

Figure 5. The SEM images of CGFSGB (a, b) and CGFSGB-S (c, d). The bright parts labelled with red are magnified and displayed on the right.

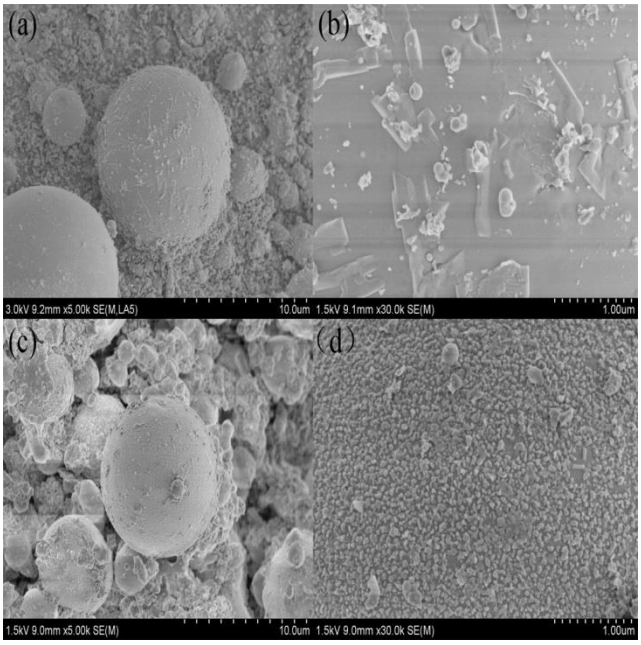

Figure 6. Wettability experiment of CGFSGB, CGFSGB-S and CGFSGB-A.

Figure 7. Stress–strain curves of neat PP and the PP composites.

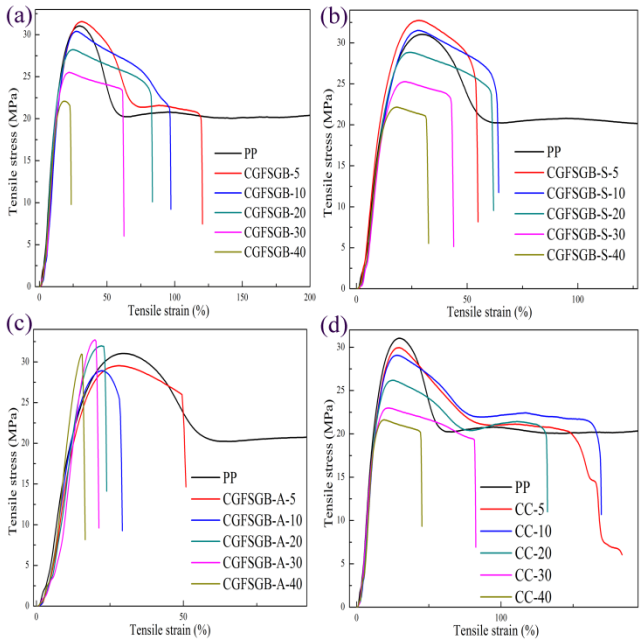

Figure 8. Dependence of tensile strength of the composites on CGFSGB, CGFSGB-S, CGFSGB-A, and CC weight fractions.

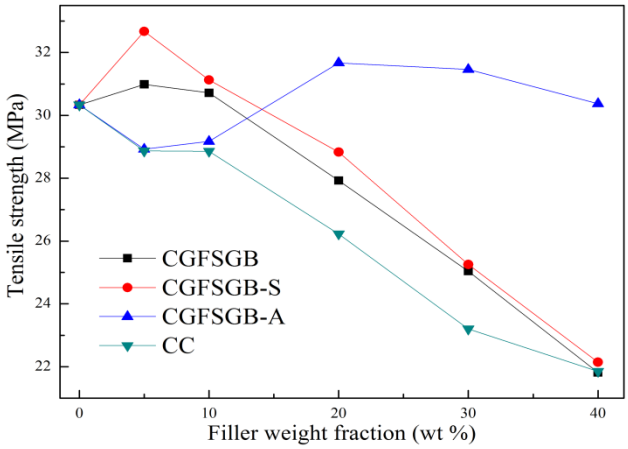

Figure 9. Turcsanyi Model for determining the tensile strength of the PP composites. *X*-axis: the volume content Φ_f of filler. *Y*-axis: $\mathrm{Ln}(\sigma/\sigma_m)-\mathrm{Ln}[(1-\Phi_f)/(1+2.318\Phi_f)]$.

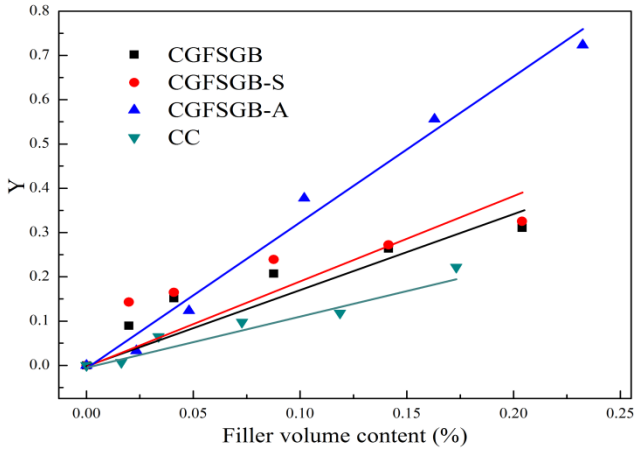

Figure 10. Dependence of the tensile elongation at break on CGFSGB, CGFSGB-S, CGFSGB-A and CC weight fraction.

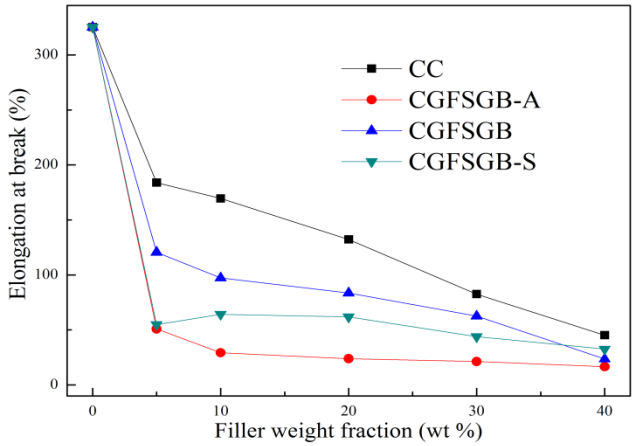

Figure 11. Linear regression analysis of the tensile elongation at break except for the pure PP.

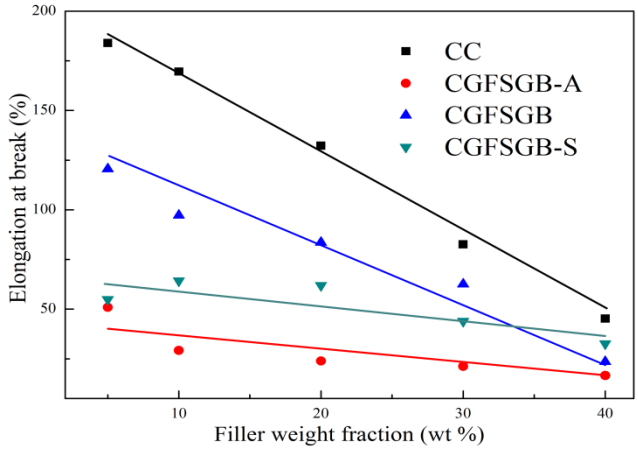

Figure 12. SEM images of tensile fracture surfaces of the PP composites: (a) PP/CGFSGB, (b) PP/CGFSGB-S, (c) PP/CGFSGB-A, (d) PP/CC.

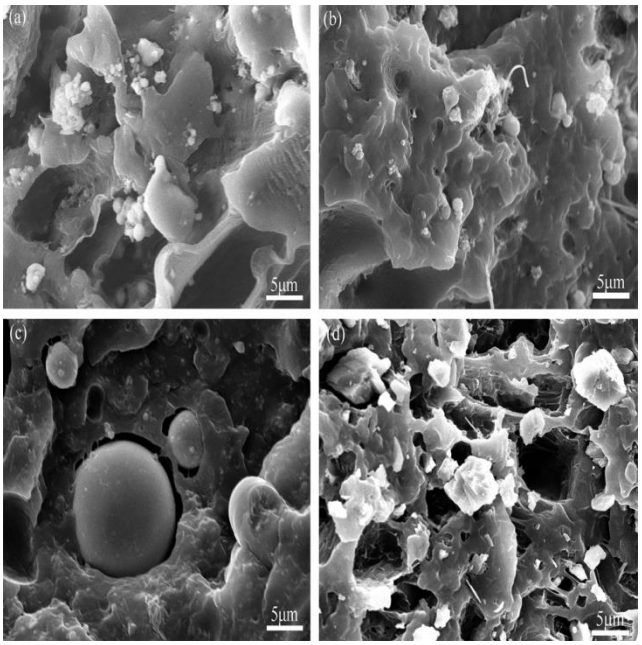

Figure 13. Thermogravimetric curves of neat PP and the PP composites.

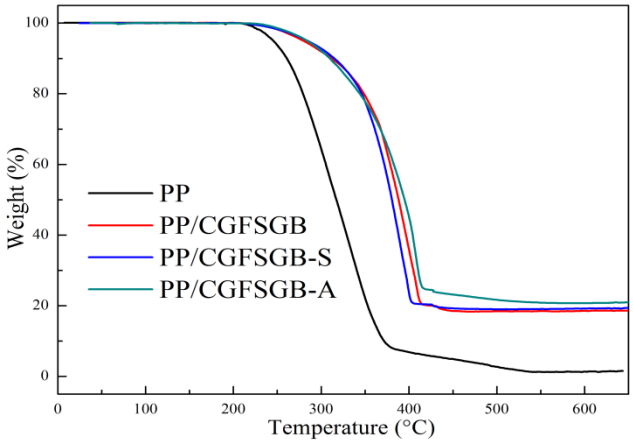

Figure 14. DSC cooling curves of pure PP and the PP/CGFSGB composites.

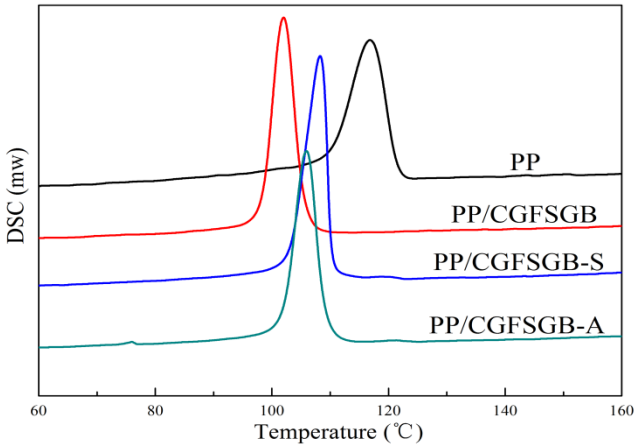

Figure 15. DSC second heating curves of pure PP and the PP/CGFSGB composites.

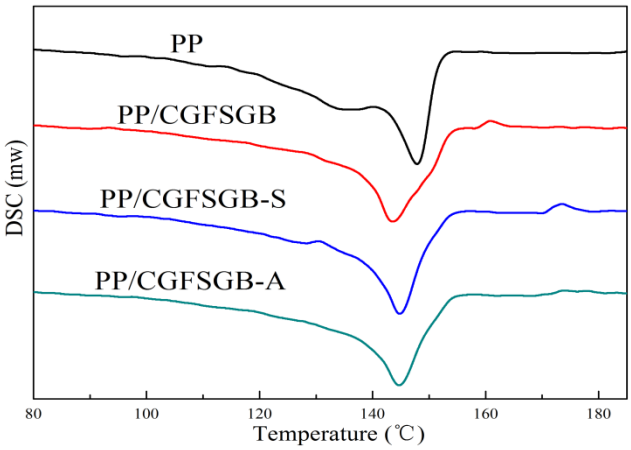

Figure 16. WAXD patterns of neat PP and the PP composites.

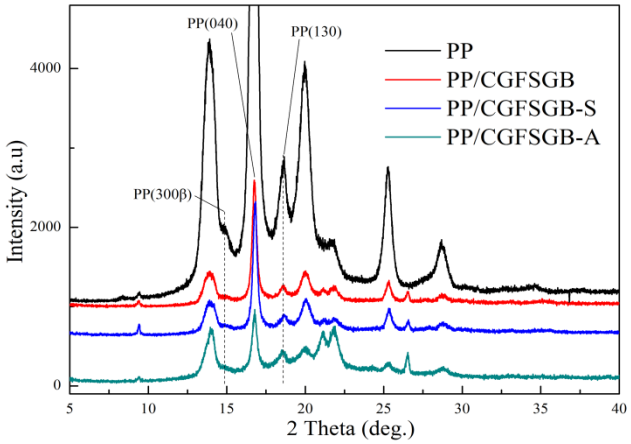

Table Ⅰ The Distribution of Particle Size of CGFSGB, CGFSGB-S, CGFSGB-A and CC

Samples	D_{10} (μm)	D_{50} (μm)	D_{90} (μm)	Dav (μm)
CGFSGB	1.507	9.228	30.092	13.161
CGFSGB-S	1.379	6.529	18.004	8.382
CGFSGB-A	2.353	9.062	21.546	10.745
CC	1.021	3.564	7.967	4.118

D_{10}, the particles with a particle size below D_{10} accounted for 10%.

D_{50}, the particles with a particle size below D_{50} accounted for 50%.

D_{90}, the particles with a particle size below D_{90} accounted for 90%.

Dav, the average volume diameter of the particles.

Table Ⅱ. Surface Area and Pore Structure of CGFSGB and CGFSGB-A

Samples	Specific surface area (m^2/g)	Pore volume (cm^3/g)	Pore size (nm)
CGFSGB	17.050	0.034	8.092
CGFSGB-A	300.463	0.238	5.415

Table Ⅲ. Elemental Analysis of the CGFAGB and CGFSGB-A by Energy Dispersive Spectrometer (EDS)

Samples	O (%)	Si (%)	Al (%)	Ca (%)	Fe (%)	Ti (%)	Na (%)
CGFSGB	40.83	18.97	9.32	19.33	4.30	0.57	0.77
CGFSGB-A	57.62	29.60	0.76	0.49	0.29	0.49	0

Table Ⅳ. Values of Parameters λ_0 and λ_1

Samples	λ_0	λ_1	R_t
PP/CGFSGB	130.5673	-2.5260	0.9555
PP/CGFSGB-S	67.7323	-0.7718	0.5998
PP/CGFSGB-A	45.1426	-0.7976	0.6349
PP/CC	208.1954	-4.0702	0.9940

Table V. Thermogravimetric Data of Neat PP and the PP Composites

Samples	T_{-10} (°C)	T_{-50} (°C)	T_{max} (°C)	Mass loss (250-400 °C) (%)	Char yield (%)
PP	260.75	317.37	540.94	86.86	1.250
PP/CGFSGB	311.90	388.07	560.20	62.26	18.57
PP/CGFSGB-S	314.75	380.49	570.00	74.54	19.32
PP/CGFSGB-A	309.83	395.04	585.24	53.42	20.90

GRAPHICAL ABSTRACT

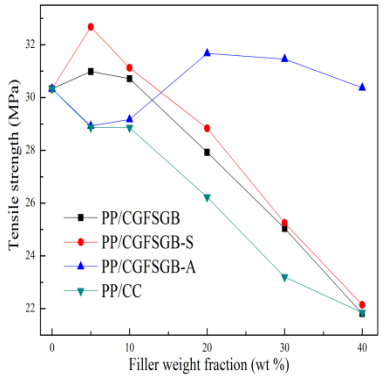

Graphical Abstract Image